A Three-Dimensional Extension of the Slope Chain Code: Analyzing the Tortuosity of the Flagellar Beat of Human Sperm

Andrés Bribiesca-Sánchez (javier.bribiesca@ibt.unam.mx)
UNAM
Adolfo Guzmán
IPN
Fernando Montoya
UNAM
Dan S. Díaz-Guerrero
UNAM
Haydeé O. Hernández
UNAM
Paul Hernández-Herrera
Autonomous University of San Luis Potosí
Alberto Darszon
UNAM
Gabriel Corkidi
UNAM
Ernesto Bribiesca
UNAM

Research Article

Keywords: 3D tortuosity, Slope Chain Code, 3D sperm flagellar beat

Posted Date: December 11th, 2023

DOI: https://doi.org/10.21203/rs.3.rs-3694554/v1

Additional Declarations: No competing interests reported.

A Three-Dimensional Extension of the Slope Chain Code: Analyzing the Tortuosity of the Flagellar Beat of Human Sperm

Andrés Bribiesca-Sánchez[1,2*], Adolfo Guzmán[3], Fernando Montoya[1], Dan S. Díaz-Guerrero[1], Haydeé O. Hernández[1,2], Paul Hernández-Herrera[4], Alberto Darszon[1], Gabriel Corkidi[1], Ernesto Bribiesca[5]

[1*]Instituto de Biotecnología, UNAM, Cuernavaca, Morelos, México.
[2]Posgrado en Ciencia e Ingeniería de la Computación, UNAM, Mexico City, Mexico.
[3]Centro de Investigación en Computación, IPN, Mexico City, Mexico.
[4]Facultad de Ciencias,UASLP, San Luis Potosí, San Luis Potosí, Mexico.
[5]Instituto de Investigaciones en Matemáticas Aplicadas y en Sistemas, UNAM, Mexico City, Mexico.

*Corresponding author(s). E-mail(s): javier.bribiesca@ibt.unam.mx;

Abstract

In the realm of 3D image processing, accurately representing the geometric nuances of line curves is crucial. Building upon the foundation set by the Slope Chain Code (SCC), which adeptly represents intricate two-dimensional curves using an array capturing the exterior angles at each vertex, this study introduces an innovative 3D encoding method tailored for polygonal curves. This 3D encoding employs parallel slope and torsion chains, ensuring invariance to common transformations like translations, rotations, and uniform scaling, while also demonstrating robustness against mirror imaging and variable starting points. A hallmark feature of this method is its ability to compute tortuosity, a descriptor of curve complexity or winding nature. By applying this technique to biomedical engineering, we delved into the flagellar beat patterns of human sperm. These insights underscore the versatility of our 3D encoding across diverse computer vision applications.

Keywords: 3D tortuosity, Slope Chain Code, 3D sperm flagellar beat

1 Introduction

In the realm of 3D computer vision and image analysis, understanding and quantifying the geometry of 3D curves extracted from images is paramount. A primary geometric characteristic of interest is tortuosity. This term embodies the overall winding nature of a curve. While it can be defined in various ways, a simple computation often used is the ratio $\tau = arclength/distance$. Despite its simplicity, this ratio encapsulates a curve's geometric complexity, making tortuosity a fundamental descriptor for numerous applications in science and engineering (Maadeed and Hassaine, 2014; Ramos et al., 2019).

Given the intricate nature of many real-world structures, more sophisticated measures of tortuosity have been explored. Especially in the biomedical realm, where the tortuosity of blood vessels and its correlation with the severity of diseases has gained significant research interest (Lisowska et al., 2014; Johnson and Dougherty, 2007; Bullitt et al., 2005).

Diving deeper into the concept of tortuosity, its essence emerges from the accumulated local degrees of bentness along a curve. In this context, the Slope Chain Code (SCC) stands out as a remarkable tool (Bribiesca, 2013). Designed to analyze 2D curves, the SCC has shown efficacy in image analysis tasks, particularly by encoding 2D curve coordinates into a chain of exterior angles or slope changes. This encoding facilitates a granular examination of a curve's local properties and provides an avenue for characterizing global features like tortuosity. Moreover, the SCC's prowess in preserving the curve's shape across various geometric transformations, such as rotations and translations, has cemented its utility in biomedical applications, notably in the treatment of diseases like retinopathy of prematurity (ROP) (Bribiesca, 2013). Yet, the inherent 2D limitation of SCC highlights the pressing need for a 3D adaptation, especially considering the rising significance of 3D analyses in understanding complex structures.

Transitioning to 3D is not without challenges. The additional degree of freedom in 3D accentuates the intricacies in characterizing curves, underscoring the need for robust methodologies. Recognizing the SCC's potential, there arises a compelling need to transition its capabilities to the 3D domain, especially given the increasing importance of 3D analyses in biomedical applications. One such critical application, which stands central to this study, is the analysis of the 3D flagellar beat of human sperm. The flagellum of sperm is a tubular structure. Analyzing how the tail twists can shed light on the intricacies of sperm motility patterns and the likelihood of such a cell fertilizing an egg. This study ventures to adapt the SCC for 3D curves, aiming to capture the complexities inherent to three-dimensional structures, and demonstrates a sample biomedical application by analyzing the flagellar beat of human sperm.

1.1 Background

In recent advancements within the domain of 3D line curve tortuosity, various methodologies have emerged. For instance, the TORT3D MATLAB code has been devised to evaluate geometric tortuosity from 3D images, notably within porous media, shedding light on the flow and transport dynamics therein (Al-Raoush and Madhoun, 2017).

Barbará-Morales et al. (2020) established a measure of tortuosity for 3D curves that was useful for detecting Alzheimer's disease in its early stages.

Recently, we introduced a measure of tortuosity for 3D curves based on the 2D-SCC tortuosity (Bribiesca-Sánchez et al., 2023). It is a method developed to evaluate the complexity of 3D polygonal curves. These are piece-wise 3D curves made up of vertices connecting straight-line segments of varying lengths. At each vertex, the absolute slope change is computed, however, it is important to consider that since the segments are not confined to a plane, the segments can tilt, so this tilting or torsion should also be measured for each vertex. The slope changes are scaled between 0 and 1, and the torsion between 0 and 0.5. The 3D-SCC tortuosity was defined as the sum of all absolute slope changes and torsions. It was shown this measure of tortuosity can be useful in different applications, emphasizing its ability to discern the 3D flagellar beat pattern of human sperm in different conditions.

The present study extends the work presented in Bribiesca-Sánchez et al. (2023) by modifying the slope change and torsion equations so that each value conveys not only the degree of twisting but its relative direction. This way we effectively adapt the Slope Chain Code to three dimensions using two chains to represent an object: a slope chain (with values ranging from -1 to 1) and a torsion chain (with values between -0.5 and 0.5). Thus the shape of the curve is preserved precisely in the encoding, and it is possible to recover the original shape. We can use this encoding to identify an object regardless of whether it is rotated, scaled, mirrored, etc. This allows us to identify local and global features of the curve, such as the tortuosity and the overall direction of the curve. Expanding the encoding in such a way allows us to delve deeper into the shape of the flagellar centerline of sperm and how its curvature fluctuates as the sperm moves.

2 Definitions

The following definitions lay the foundation for the methodologies and analyses explored in this study. By establishing a clear understanding of these foundational concepts, we aim to ensure clarity in the subsequent sections.

Definition 1 (3D Polygonal Curve)**.** *A 3D polygonal curve is a piece-wise linear curve in a 3D space, comprised of a sequence of vertices connected by straight-line segments.*

A sample 3D polygonal curve is illustrated in Fig. 1(a). We refer to vertices that connect a pair of segments as *inner vertices*, while those connected to a single segment are referred to as *outer vertices*. For open curves with m segments, there will be $n = m - 1$ inner vertices. In the case of closed curves, where inherently no outer vertices exist, $n = m$.

Definition 2 (Tangent vector)**.** *Given two consecutive vertices $\vec{X}_j$ and $\vec{X}_{j+1}$, the tangent vector $\vec{T}_j$ is defined as the vector pointing from vertex X_j to vertex X_{j+1}, mathematically represented as* $\vec{T}_j = \frac{\vec{X}_{j+1} - \vec{X}_j}{||\vec{X}_{j+1} - \vec{X}_j||}$.

Definition 3 (Normal vector)**.** *The normal vector $\vec{N}_j$ is a vector perpendicular to the segments intersecting at vertex j. Mathematically, it is represented as $\vec{N}_j = \frac{\vec{T}_{j-1} \times \vec{T}_j}{||\vec{T}_{j-1}|| \, ||\vec{T}_j||}$.*

The normal vector defines a plane parallel to segments intersecting at vertex j, which is helpful for the assessment of torsion. This is known as the osculating plane.

Our encoding uses 2 chains to represent a curve: a slope chain, which is the sequence of slope changes at each vertex, and a torsion chain which represents the tilting difference.

Definition 4 (Slope Change)**.** *The slope change α_j at vertex j is the normalized angle, in the range (-1,1), formed by two adjacent line-segments incident on vertex j. It quantifies the local deviation from a straight path at the vertex.*

Slope change, visualized in Fig. 1, encapsulates the local bending of the curve, with 0 indicating the two segments follow a linear path, and 1 signifying that the segments have opposite directions. Fig 1b shows the range of slope changes.

Definition 5 (Torsion)**.** *Torsion β_j at vertex j is defined as the normalized angle, within [-0.5, 0.5], representing the amount a segment s_i needs to roll along segment s_j to be co-planar with s_{j+1}. Vertex i is the most recent non-co-linear vertex before j.*

Torsion, essentially, gauges the tilt of a curve segment sequence. It requires at least three segments for computation and is thus absent for the first inner vertex in open curves. For a curve, the number of slope changes and torsions are denoted as n_α and n_β respectively, with $n_\alpha = n$ and $n_\beta = n$ for closed curves, and $n_\beta = n - 1$ for open ones. Further details on torsion computation are elaborated in Section 2.2.

2.1 Computing Slope Changes in a 3D Polygonal Curve

We assume that the vertices of a 3D polygonal curve have already been extracted from the source. To compute the slope chain of a 3D curve we must select an initial vertex (indicated by a red sphere in Fig. 1(a)) and travel along the sequence of vertices. We aim to adapt the ability of the slope chain code in 2D to describe the local curvature and relative direction to 3D. For this reason, we modified the expression given for the slope changes in Bribiesca-Sánchez et al. (2023) including a sign that switches whenever a sequence of segments is concave. Mathematically, the slope change α_j is

$$\alpha_j = sign_{\alpha_j} \arccos\left(\frac{\vec{T}_j \cdot \vec{T}_{j+1}}{||\vec{T}_j|| \, ||\vec{T}_{j+1}||}\right)/\pi, \tag{1}$$

The sign of the first slope change can be set arbitrarily. In this work, we will always consider it 1. For the following angles

$$sign_{\alpha_j} = \begin{cases} sign_{\alpha_{j-1}} & \text{if } (\vec{T}_i \cdot \vec{v}_i)(\vec{T}_{j+1} \cdot \vec{v}_i) < 0, \\ (-1) sign_{\alpha_{j-1}} & \text{otherwise.} \end{cases}$$

where $\vec{v}_i = \vec{N}_i \times \vec{T}_i$. $\vec{T}_i$ indicates the local forward direction, serving as a provisional x-axis, and $\vec{v}_i$ serves as the y-axis. If T_{i-1} and T_j move towards opposite sides of the "x" plane the sign remains the same, since the curve is curling more, whereas if

they end up on the same side of the "x" axis the sign is negative. Thus, the arccosine measures the absolute slope change and the sign remains the same if the sequence rotates in the same direction, forming a C-shape, and the sign changes if the sequence of segments forms an S-shape.

Fig. 1(c) shows the computation of the first slope change. Fig. 1(d) illustrates all computed slope changes of the curve, with subsequent slope changes computed considering the next pair of 3D straight-line segments. Notice that the segments of the curve do not need to be of the same length.

2.2 Calculating Torsions in a 3D Polygonal Curve

Torsions in a 3D polygonal curve are derived by determining the angle between planes containing segments, connected at vertices i and j. Again we modified the equation from Bribiesca-Sánchez et al. (2023) to allow positive or negative signs depending on whether the plane tilts upwards or downwards from the plane containing the previous segments, using the right-hand rule as a frame of reference. The torsion at vertex i is expressed as:

$$\beta_j = \arcsin\left(\frac{\vec{T}_i \cdot (\vec{N}_i \times \vec{N}_j)}{||\vec{N}_i||\,||\vec{N}_j||}\right)/\pi, \tag{2}$$

where vertex i and j are connected by a straight path of one or more segments.

Fig. 2 illustrates the osculating planes used to compute the torsion of the 3D polygonal curve displayed in Fig 1(a). As the first vertex of an open polygonal curve lacks torsion, the computation starts from the second vertex, proceeding sequentially to subsequent vertices. Thus torsion chain of the curve in Fig. 2 is: [0. 0. -0.5 0.2 0.25 0.1 -0.3 -0.]

When slope changes are zero, the algorithm to compute torsions becomes slightly intricate since a tangent plane could assume any orientation, resulting in a lost torsion reference frame. Thus, the algorithm utilizes Remark 1 to retain the last corner vertex i as a reference for the torsion of vertex j. Additionally, if the initial vertex of an open curve is zero, an initial plane of reference for torsion cannot be immediately established due to the vectors being co-linear. In this scenario, we set $\beta_1 = 0$. This is repeated as $\beta_{j+1} = 0$ for every vertex j until $\alpha_j \neq 0$ is found, ultimately allowing the establishment of the tangent plane. The torsion at vertex $j+1$ will be determined between the segments at vertex j and $j+1$.

Remark 1. *For any vertex $j = 1, \ldots, n$; if $\alpha_j = 0$, then $\beta_j = 0$.*

3 Properties

3.1 Uniqueness of Encoding

Our encoding methodology significantly on our previous work Bribiesca-Sánchez et al. (2023) by ensuring each curve has a unique encoding. This unique representation relies on one key condition: when comparing two curves, the corresponding segments in each curve should match in length. By incorporating directional information in the slope and torsion calculations, our method accurately captures the distinct geometric

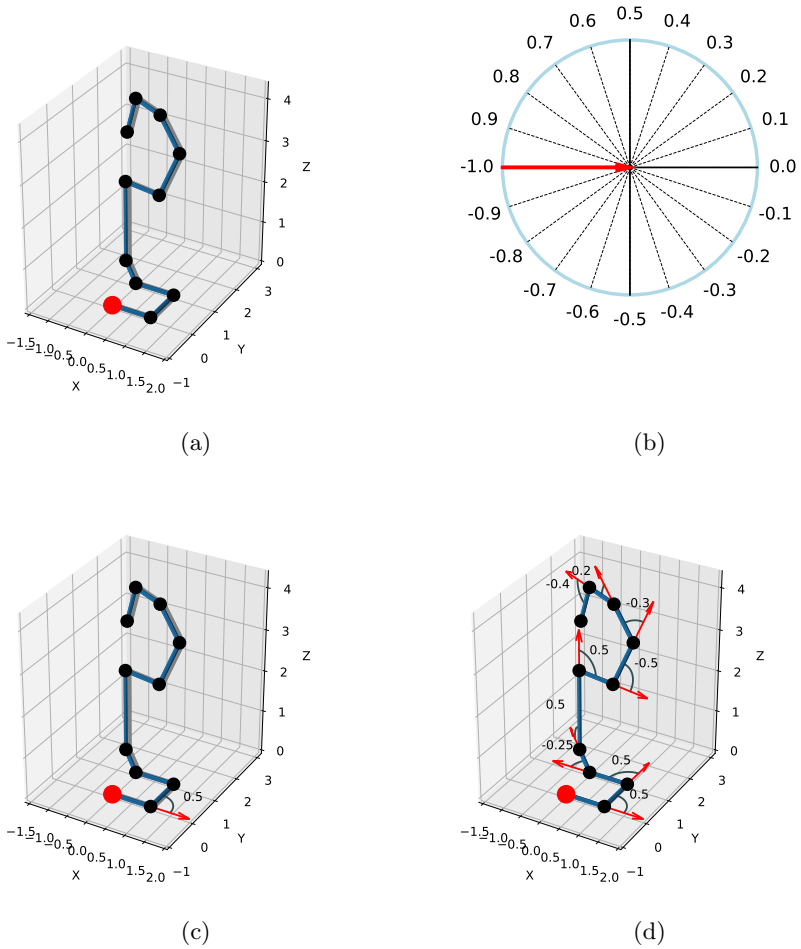

Fig. 1: Computation of the slope change: (a) Sample 3D polygonal curve, (b) slope change range $(-1, 1)$, (c) Computation of the slope first slope change, and (d) computation of all the slope changes of the curve. The slope chain of this curve is: [0.5 0.5 -0.25 0.5 0.5 -0.5 -0.3 -0.2 -0.4].

characteristics of each curve. This unique encoding is crucial for distinguishing between different curves, enhancing the precision and usefulness of our method in fields like computer vision and biomedical imaging, where accurate curve characterization is vital.

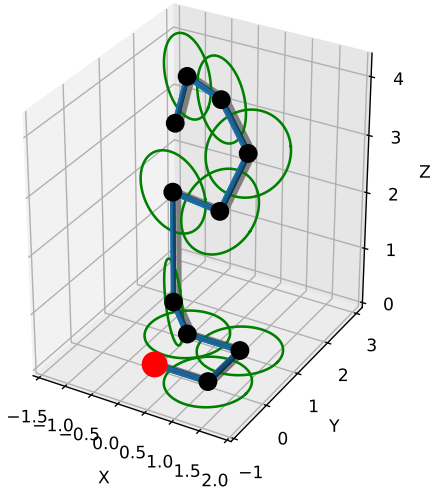

Fig. 2: Osculating planes. The torsion is the tilting angle between these planes.

3.2 Translational, Rotational, and Scale Invariance

The 3D encoding exhibits invariance under translations, rotations, and uniform scaling transformations. This stems from the relative nature of the slope changes and torsions computed between contiguous straight-line segments. Figure 3 illustrates these invariances through various transformations applied to the 3D polygonal curve depicted in Figure 1(a), all of which retain the same encoding.

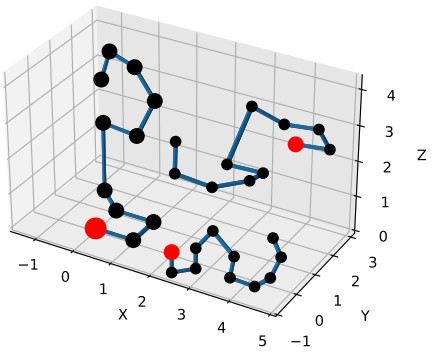

Fig. 3: Rotated, translated, and scaled polygonal curve. All of them have the same slope and torsion chains.

3.3 Mirror Imaging

The symmetry of a mirror transformation leaves the slope chain unaltered, while the torsion chain's signs invert. This is because the first slope change has a fixed sign (positive in our work) but the torsion must invert to comply with the right-hand rule. This property is illustrated in Figure 4.

3.4 Starting Point

If a curve is traveled in reverse order, its torsion chain will be the same but in reverse order and with inverted signs. The slope chain will also reverse and the signs will be inverted if the first and last signs of the original chain do not match.

Furthermore, in a closed curve any vertex can be chosen as the starting vertex and the encoding will be the same, but shifted and possibly with inverted signs.

Figures 5(a) and (b) elucidate this invariance for an open curve, while Figures 5(c) and (d) extend this illustration to a closed curve.

3.5 Consistency with SCC-2D

If a curve is planar, i.e. all of its torsions are 0, the slope chain will be equal to the 2D slope chain code (or its mirror image if the first slope change is clockwise).

3.6 Accumulated Angles

A helpful feature of the slope chain code is the ability to obtain complex properties of a curve by simply adding their values. In 3D the sum of slope changes and torsions, signed and absolute can provide helpful insights about the structure of a curve that contribute to their analysis and classification.

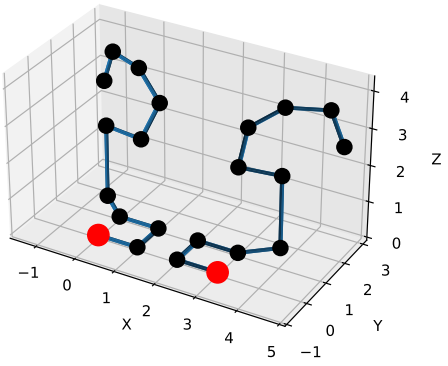

Fig. 4: Mirrored curve. Both curves have the same slope chain and opposite-signed torsions.

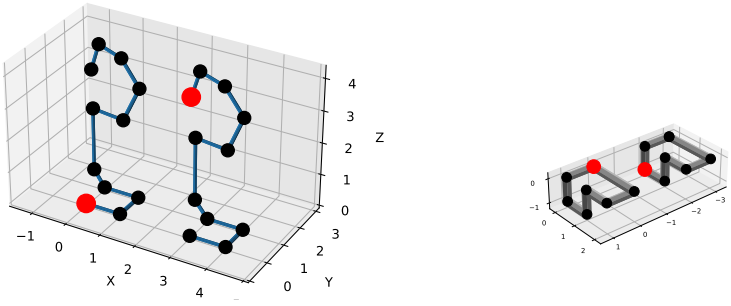

(a) (b)

Fig. 5: Polygonal curves with different starting points. (a) When the 3D polygonal curve shown in Fig. 1(a) is traveled in reverse, its slope and torsion chains are reversed and their signs switch. (b) closed curve with different starting points.

Definition 6 (Accumulated slope change)**.** *The accumulated slope change of a 3D polygonal curve is the sum of all its slope changes and it is denoted as:*

$$\alpha_{Abs} = \Sigma_0^n \alpha_j \quad \text{for open curves} \tag{3}$$

$$\alpha_{Acc} = \Sigma_1^n \alpha_j \quad \text{for closed curves}$$

Definition 7 (Accumulated absolute slope change)**.** *The accumulated absolute slope change of a 3D polygonal curve is the sum of the absolute values of all its slope changes and it is denoted as:*

$$\alpha_{Abs} = \Sigma_0^n |\alpha_j| \quad \text{for open curves} \tag{4}$$

$$\alpha_{Abs} = \Sigma_1^n |\alpha_j| \quad \text{for closed curves}$$

Remark 2. *A 3D polygonal curve is a straight line if and only if its accumulated absolute slope change is 0.*

Definition 8 (Slope Direction Factor (SDF))**.** *The Slope Direction Factor is given by*

$$SDF = \frac{\alpha_{Acc}}{\alpha_{Abs}} \tag{5}$$

It is a descriptor that is 1 if all slope changes are positive, -1 if all slope changes are negative, and 0 if they balance out.

The accumulated slope change of the polygonal curve in Fig. 1(a) is $0.5 + 0.5 - 0.25 + 0.5 + 0.5 - 0.5 - 0.3 - 0.2 - 0.4 = 0.35$. The accumulated slope change of the polygonal curve in Fig. 1(a) is 3.65. Thus its SDF is 0.35/3.65.

Definition 9 (Accumulated torsion)**.** *The accumulated torsion of a 3D polygonal curve is the sum of its torsions, i.e.:*

$$\beta_A cc = \Sigma_1^n \beta_j \tag{6}$$

Definition 10 (Accumulated absolute torsion)**.** *The accumulated absolute torsion of a 3D polygonal curve is the sum of its torsions, i.e.:*

$$\beta_{Abs} = \Sigma_1^n |\beta_j| \tag{7}$$

The accumulated torsion of the curve in Fig. 2(a) is $-0.5+0.2+0.250.1-0.3 = -.25$. Its accumulated torsion is 1.35.

Remark 3. *A polygonal curve is planar if and only if its accumulated torsion is 0.*

4 3D Slope Chain Code Tortuosity

Definition 11 (3D-SCC Tortuosity)**.** *The 3D-SCC tortuosity, denoted by τ, of a polygonal curve is computed as the cumulative sum of the absolute slope changes and absolute torsions occurring between adjacent line segments, mathematically represented as:*

$$\tau = \alpha_{Abs} + \beta_{Abs} \tag{8}$$

This derives from the definition given in our previous work (Bribiesca-Sánchez et al., 2023), but is adapted to consider the absolute value, which would have been redundant in that work since all angles were positive because they were not directional. In Figure 1(a), the computed slope and torsion values aggregate to $\tau = 3.65 + 1.35 = 5$.

4.1 Invariance

Due to the properties of the 3D encoding, the 3D SCC tortuosity is invariant under rotation, translation, scale, mirror imaging, and starting point, since the absolute values do not change.

4.2 Extrema of 3D Tortuosity

From this section on, we address 3D polygonal curves with equal-sized segments exclusively. A 3D polygonal curve manifests the minimum tortuosity value of $\tau = 0$ when all its slope changes are null. Conversely, the maximum value of tortuosity is reached when all slope changes approximate ± 1 and every torsion angle measure ± 0.5. This yields an accumulated slope of $\sim n$ and an accumulated torsion of $\frac{n_t}{2}$. Therefore, the tortuosity of any given curve is bounded within the interval $[0, n + \frac{n_t}{2})$.

4.3 Normalized 3D Tortuosity

The preceding section delineates how the maximum tortuosity value escalates with the number of vertices within the polygonal curve. To surmount this, we propose a normalized tortuosity measure that facilitates a standardized comparison across curves with disparate vertex counts. This normalization is not only conducive to comparative analysis but also aligns well with the prerequisites of numerous regression and classification models in which bounded descriptor values are preferred.

Definition 12 (Normalized Tortuosity)**.** *The Normalized Tortuosity, denoted τ_N, is derived by scaling the raw tortuosity τ by the maximum possible tortuosity given the number of vertices, expressed as:*

$$\tau_N = \frac{\tau}{n + \frac{n_t}{2}}. \tag{9}$$

This normalization ensures that the tortuosity measure lies within the continuous range $[0, 1)$. For instance, the left curve in Figure 6 exhibits the minimum normalized tortuosity value of zero, while the right curve approaches the maximum value of one.

The normalized tortuosity of the curve described in Fig. 1(a) is $5/(9 + 4) = 0.38$

Overall this encoding can accurately depict the shape of 3D curves directly and through the computation of descriptors such as the 3D-SCC tortuosity and normalized tortuosity, stand out as robust descriptors of the geometric essence of 3D curves. The encoding is impervious to alterations in translation, size, and other extrinsic factors. Their utility extends to ranking curves based on tortuosity, aiding in shape comparison, and classification. Moreover, it promises significant advancements in detecting and analyzing the geometry of 3D tubular structures and curves prevalent in veins, respiratory airways, arteries, and architectural infrastructures, among others.

5 Results

5.1 Analysis of closed curves using their tortuosity

The study of closed curves finds diverse applications in topology, graph theory, fluid mechanics, and chemistry. In these domains, the ability to quantitatively describe and

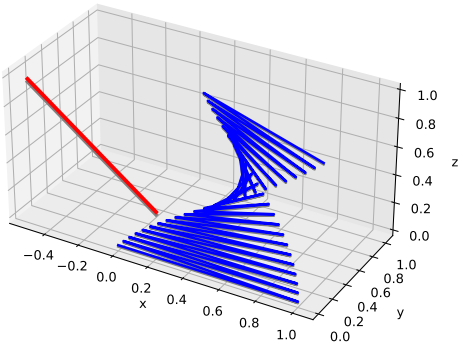

Fig. 6: 3D polygonal curves exhibiting minimal and maximal tortuosity.

analyze curve shapes - a process often reliant on visual interpretation - is invaluable. Descriptors extracted from the 3D SCC can transform these qualitative observations into quantitative data, facilitating the classification and ranking of various patterns.

Figure 7 presents several closed curves comprised by different numbers of vertices n, each exhibiting distinct characteristics. Accompanying Table 1 quantifies their properties, including accumulated slope, accumulated torsion, and overall tortuosity. Fig. 7(a) displays a simple knot. This curve, characterized by its smoothness, registers the lowest tortuosity among the samples. Its simplicity is reflected in its minimal tortuosity. Figure 7(b) Exhibits high values in both accumulated slope and torsion, this curve is markedly tortuous. Its complexity is evident in its intricate structure. Fig. 7(c)): Has a tilting, zigzagging nature which amplifies both its accumulated slope and torsion, resulting in the highest normalized tortuosity - particularly notable given its lower number of vertices compared to Fig. 7(b). Finally, Fig. 7(d) is somewhat planar, leading to a low accumulated torsion, but the curve's loops contribute to its significant tortuosity. The ranking from least to most tortuous, based on our analysis, is as follows: (a), (d), (c), and (b).

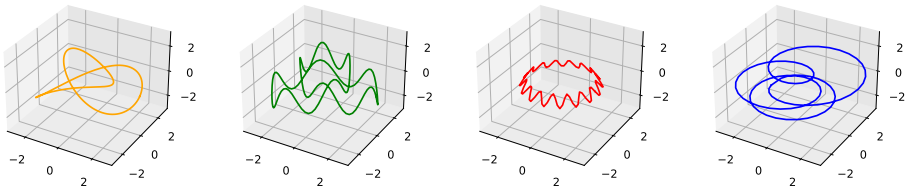

(a) (b) (c) (d)

Fig. 7: Sample closed 3D polygonal curves illustrating varying degrees of tortuosity.

Table 1: Quantitative analysis of the 3D polygonal curves in Fig. 7. The table enumerates each curve's vertices (n), accumulated slope (S), accumulated torsion (T), tortuosity measure (τ), and normalized tortuosity (τ_N).

Curve	n	Accum. Abs. Slope	Accum. Abs. Torsion	Tortuosity (τ)	Norm. Tortuosity (τ_N)
(a)	200	4.44	1.61	6.05	0.02
(b)	150	15.4	15.6	31.0	0.14
(c)	100	26.13	7.24	33.37	0.22
(d)	100	7.99	0.7	8.69	0.06

A key feature to highlight is that the accumulated absolute slope of the knot displayed in curve (a) is 4.44. In general, it can be stated that for any non-trivial knot, this value must be greater or equal to 4. This is a discrete, SCC adaptation of the Fary-Milnor theorem, which states that any non-trivial knot has a total curvature of at least 4π (Milnor, 1950). Thus this descriptor can be helpful criteria in detecting unknots.

Theorem 1 (3D SCC Fary-Milnor Theorem)**.** *Any non-trivial knot's accumulated absolute slope change is at least* 4*.*

5.2 Analysis of the 3D flagellar beat of human sperm

To demonstrate the potential real-world applications of this 3D encoding, we highlight its utility in identifying 3D beating patterns in the tail of human sperm. In their pursuit of the egg, human spermatozoa use a complex, three-dimensional beat of their flagellum to navigate through the reproductive tract. Identifying flagellar beat patterns is crucial to understanding whether a sperm can fertilize the egg, however, their rapid, intricate, and three-dimensional nature contributes to obscure the true nature of these patterns. Furthermore, as spermatozoa navigate through their medium, they translate and rotate along their movement axis. This rotation introduces additional complexities in the analytical exploration of freely-swimming sperm. If this rotation is neglected, artifacts can emerge in measurements. Therefore, the use of rotationally invariant descriptors becomes essential for an accurate evaluation of the flagellar beat. We believe that 3D SCC can provide valuable insight into identifying the flagellar beating patterns of fertile human sperm.

The 3D flagellar beat of 90 freely swimming human sperm was analyzed. During each experimental session, an individual, freely-swimming spermatozoon was imaged for 3 s utilizing an experimental apparatus consisting of an inverted microscope equipped with a piezoelectric device (Hernandez-Herrera et al., 2018; Corkidi et al., 2008). This device induced vibrations in the objective along the z-axis at a frequency of 90 Hz, spanning a vertical range of 20 μm, while a high-speed camera simultaneously captured images at a rate of 8000 frames per second. Consequently, images obtained at various heights were systematically aligned to reconstruct the 3D+time recorded volume. The flagellum's centerline was segmented from each 3D frame using a semi-automated algorithm designed to find a path, connecting the sperm head and distal point of the flagellum via approximately 400 3D linear segments of equal lengths.

The flagellum was smoothed with a least squares B-spline to eliminate high-frequency noise in the centerline coordinates. This approach generated a 3D open polygonal curve. Further details on the data acquisition and segmentation methodologies were discussed in Hernandez-Herrera et al. (2018).

5.2.1 3D Slope Chain Analysis

Analyzing the 3D slope chains of the flagellum can provide interesting information on the flagellar beat since they allow us to quantitatively monitor how the curvature travels along the flagellum while the sperm swims. The slope chain represents how much the flagellum bends in each of its regions, and in which relative direction. Thus Fig. 8(a) shows the flagellum of a sperm with a slow flagellar beat over 12/90 s. The color represents the value of the slope chain in that region. Thus, we can observe that regions with a significant bend correspond with high values in the slope chain (red regions). The flagellum of this curve is very smooth with long quasi-linear regions (green) and a main curvature region (red) traveling slowly from the neck towards its endpoint with the whip-like motion of the flagellum. A spermatozoon with a more tortuous flagellar beat is shown in Fig. 8(b) during a span of 5/90 s. In this case, the flagellum has multiple critical points (red regions), contributing to its high tortuosity. Notice that the slope changes are always positive (no regions of the flagellum are tainted blue). This is because the Slope Direction Factor is high for the recorded cells, averaging 0.88. This indicates that the flagellum is a helix-like structure.

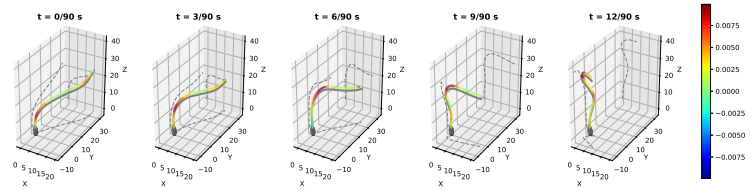

(a)

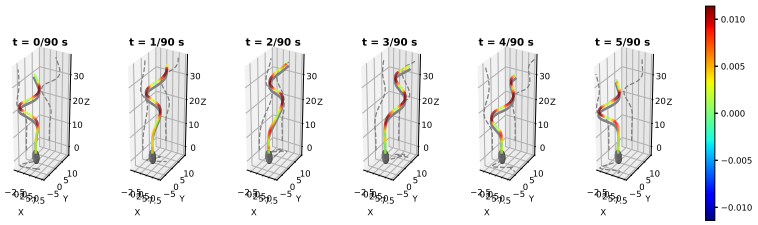

(b)

Fig. 8: Slope changes of the flagellar beat of (a) a human sperm elapsing 12/90 s with low tortuosity and (b) Slope changes of the flagellar beat of a highly tortuous human spermatozoon elapsing 8/90 s. The color represents the slope changes.

5.2.2 3D-SCC flagellar tortuosity

Upon obtaining the slope and torsion chains of the flagellum at each time frame of the 90 analyzed cells, we computed their 3D-SCC tortuosity. The average tortuosity of each experiment ranged from 3.4 to 5.2 (normalized tortuosity between 0.033 and 0.050). Fig. 9 illustrates the flagellar beat of 6 sample sperm over 0.25s, with increasing tortuosity values. Figures 9(a-b) each display a spermatozoon with low flagellum tortuosity (Average $\tau = 3.6$). Fig. 9(b-c) each show a sperm with medium tortuosity (Average $\tau = 4.1$). Finally, a cell with high flagellar tortuosity ($\tau = 5.1$) is shown in Fig. 9(d-e). As the tortuosity increases, the flagella tend to be less smooth and more crooked.

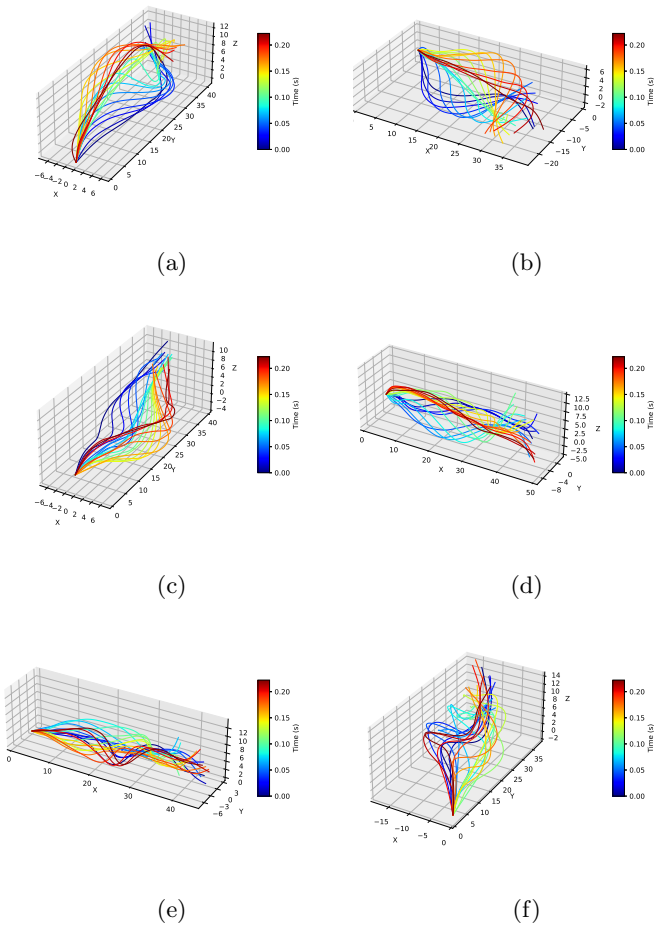

Fig. 9: 3D flagellar beat elapsing 0.25 of (a-b) sperm with low flagellar tortuosity, (c-d) sperm with medium flagellar tortuosity, and (e-f) a sperm with high flagellar tortuosity.

5.3 3D-SCC tortuosity of the sperm trajectory

Another interesting approach to analyzing sperm motility is encoding the 3D trajectory of the sperm and computing its tortuosity. Fig. 10(a) shows the 3D trajectory of a sample sperm with low tortuosity. It has very smooth wide movement as the sperm moves in a linear path. Wide lateral movement is known to be an important feature in the motility of fertile cells Marín-Briggiler et al. (2021). In contrast, Fig. 10 shows the 3D path of a sperm with high 3D-SCC tortuosity, which has very short and sudden motions as it swims.

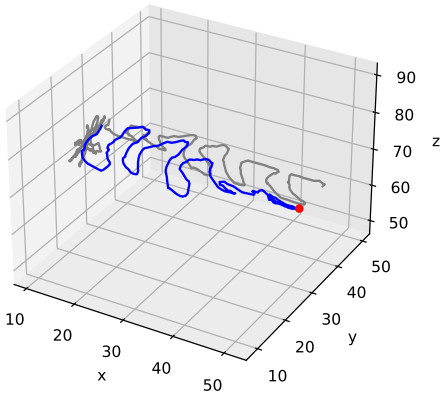

(a)

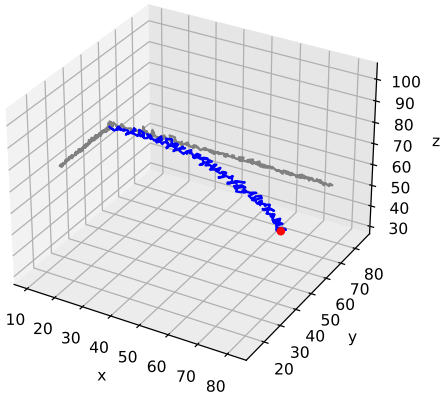

(b)

Fig. 10: 3D trajectories of sperm with (a) low 3D-SCC tortuosity and (b) high 3D-SCC tortuosity. The red dot indicates the start of the trajectory.

6 Conclusion

We developed an encoding for 3D curves based on the Slope Chain Code which uses two chains in parallel to represent it: a slope chain and a torsion chain. It is invariant under changes in size, rotation, and translation, and robust to mirror imaging and starting point. It allows the extraction of features such as tortuosity, accumulated angles, and direction factors. We showed the potential of this encoding in the analysis of knots and closed curves. Furthermore, we exemplified the biomedical application of this encoding showing its potential in the analysis of the 3D flagellar center-line human sperm. The variability in 3D-SCC tortuosity highlighted the diverse range of flagellar beat patterns in human sperm. The high Slope Direction Factor indicated a predominantly helix-like flagellar motion among the sperm. We believe these could be useful features in medical systems to identify fertile cells since they are statistically significant, in contrast to their 2D counterparts. While we demonstrated significant findings in the context of reproductive biology, the potential applications of our 3D-SCC method extend into other areas of computer vision and 3D curve analysis. This versatility opens up avenues for future research in medical imaging, robotics, and more. Future work could focus on refining the encoding method to enhance its accuracy and exploring its application in other complex 3D structures beyond biological systems.

Declarations

Ethical Approval

Young healthy donors supplied human spermatozoa with informed written consent and the supervision of the Bioethics committee of the Instituto de Biotecnología, UNAM. The semen samples fulfilled the World Health Organization (WHO) requirements.

Funding

This work was supported by DGAPA PAPIIT (IN105222), Chan Zuckerberg Initiative DAF Grant (2020-225643), and CONAHCYT (PhD scholarship).

Data availability

Data is available upon reasonable request to the corresponding author.

References

Al-Raoush, R. I. and Madhoun, I. T. (2017). Tort3d: A matlab code to compute geometric tortuosity from 3d images of unconsolidated porous media. *Powder Technology*, 320:99–107.

Barbará-Morales, E., Pérez-González, J., Rojas-Saavedra, K. C., and Medina-Bañuelos, V. (2020). Evaluation of brain tortuosity measurement for the automatic multimodal classification of subjects with alzheimer's disease. *Computational Intelligence and Neuroscience*, 2020.

Bribiesca, E. (2013). A measure of tortuosity based on chain coding. *Pattern Recognition*, 46:716–724.

Bribiesca-Sánchez, A., Guzmán, A., Darszon, A., Corkidi, G., and Bribiesca, E. (2023). A measure of tortuosity for 3d curves: Identifying 3d beating patterns of sperm flagella. *Lecture Notes in Computer Science (including subseries Lecture Notes in Artificial Intelligence and Lecture Notes in Bioinformatics)*, 14062 LNCS:363–374.

Bullitt, E., Zeng, D., Gerig, G., Aylward, S., Joshi, S., Smith, J. K., Lin, W., and Ewend, M. G. (2005). Vessel tortuosity and brain tumor malignancy: A blinded study. *Academic Radiology*, 12:1232–1240.

Corkidi, G., Taboada, B., Wood, C., Guerrero, A., and Darszon, A. (2008). Tracking sperm in three-dimensions. *Biochemical and Biophysical Research Communications*, 373(1):125–129.

Hernandez-Herrera, P., Montoya, F., Rendón-Mancha, J. M., Darszon, A., and Corkidi, G. (2018). 3-d + t human sperm flagellum tracing in low snr fluorescence images. *IEEE Transactions on Medical Imaging*, 37:2236–2247.

Johnson, M. J. and Dougherty, G. (2007). Robust measures of three-dimensional vascular tortuosity based on the minimum curvature of approximating polynomial spline fits to the vessel mid-line. *Medical Engineering and Physics*, 29:677–690.

Lisowska, A., Annunziata, R., Loh, G. K., Karl, D., and Trucco, E. (2014). An experimental assessment of five indices of retinal vessel tortuosity with the ret-tort public dataset. *2014 36th Annual International Conference of the IEEE Engineering in Medicine and Biology Society, EMBC 2014*, pages 5414–5417.

Maadeed, S. A. and Hassaine, A. (2014). Automatic prediction of age, gender, and nationality in offline handwriting. *Eurasip Journal on Image and Video Processing*, 2014.

Marín-Briggiler, C. I., Luque, G. M., Gervasi, M. G., Oscoz-Susino, N., Sierra, J. M., Mondillo, C., Salicioni, A. M., Krapf, D., Visconti, P. E., and Buffone, M. G. (2021). Human sperm remain motile after a temporary energy restriction but do not undergo capacitation-related events. *Frontiers in Cell and Developmental Biology*, 9:777086.

Milnor, J. W. (1950). On the total curvature of knots. *Annals of Mathematics*, 52:248.

Ramos, L., Novo, J., Rouco, J., Romeo, S., Álvarez, M., and Ortega, M. (2019). Computational assessment of the retinal vascular tortuosity integrating domain-related information. *Scientific Reports*, 9:19940.